Electronic Supplementary Information (ESI)

1T/1T'-dominated WSe_2 with stabilized oxygen dopants for efficient and durable hydrogen evolution

Zhuxing Sun[a†], Yiwen Wang[a†], Junyu Lang[a], Mengfei Yang[a], Fangming Jin[a*], Yun Hang Hu[b*]

[a] School of Environmental Science and Engineering, Shanghai Jiao Tong University, Shanghai, 200240, China

[b] Department of Materials Science and Engineering, Michigan Technological University, Houghton, MI 49931, United States

Corresponding author E-mails: fmjin@sjtu.edu.cn, yunhangh@mtu.edu

† Both authors contribute equally to this work.

Experimental Details

Material Synthesis

Hybrid-phase WSe_2 (*hp*-WSe_2) was synthesized by a one-pot solvothermal strategy. Precisely 2 mmol SeO_2 powder were dissolved in 30 mL DMF and continuously stirred at 50 °C to form a homogenous solution. After that, 1 mmol of WCl_6 was added to the mixture. After that, a graphite rod (with a diameter of 3 mm and a length of 50 mm) was soaked in the as-prepared precursor mixture for 12 h. Then, the graphite rod and the mixture were transferred into a 50 mL autoclave and heated at 200 ℃ for 12 h. The autoclave was cooled down to the room temperature naturally. Thus, a graphite rod grown with *hp*-WSe_2 catalysts was obtained. The sample was then rinsed several times by deionized water and ethanol to remove the residuals and kept in deionized water before tests.

Co/*hp*-WSe_2 and Co/P/*hp*-WSe_2 were synthesized via similar solvothermal processes, except that $Co(NO_3)_2$ and KH_2PO_4 were additionally introduced to the precursor solution. Respectively, 0.1 mmol of $Co(NO_3)_2$ and 0.9 mmol WCl_6 were added to the mixture of 2 mmol SeO_2 and 30mL DMF for Co/*hp*-WSe_2; for Co/P/*hp*-WSe_2, 0.1 mmol $Co(NO_3)_2$, 0.1 mmol KH_2PO_4 and 0.9 mmol WCl_6 were added to the mixture of 1.9 mmol SeO_2 and 30 mL DMF.

Characterization

The microscopic morphologies of the as-obtained materials were investigated by with field emission scanning electron microscopy (SEM, Sirion 200/IAC) and transmission electron microscopy (TEM, FEI Tecnai G2 F20). The crystal phases of the samples were collected on an X-ray diffractometer (XRD-6100, LabX, SHIMADZU Ltd. Japan) with Cu-K radiation. The chemical state of the elements in the samples were studied by X-ray photoemission spectroscopy (XPS, Thermo Fisher Scientific Escalab 250Xi) with a monochromatic Al Kα source. The ratios of different elements in the catalysts are measured by inductively coupled plasma-mass

spectroscopy (ICP-MS, Thermo Fisher Scientific, ICP Q). The BET surface area was acquired on a surface area and porosity analyzer (Micromeritics ASAP 2020 PLUS HD88, USA).

Electrochemical Measurements

Electrochemical measurements were performed in a 3-electrode system using an electrochemical station (CHI 760E, CH instruments, Inc., USA). The electrolyte was 0.5 M H_2SO_4. The as-prepared 3D electrodes (3 mm in diameter) were used directly as the working electrode with an immersed length of 21 mm. An Ag/AgCl electrode and a graphite electrode were used as the reference and counter electrodes, respectively. The potential was calibrated with respect to reversible hydrogen electrode (RHE), i.e., $E_{RHE}=E_{Ag/AgCl}$ + 0.1976 V in 0.5 M H_2SO_4. Linear sweep voltammetry (LSV) experiments were preformed from 0 to -0.4 V (vs. RHE) with a sweep rate of 0.5 mV/s to obtain the polarization curves. Since the electrochemical cell contains series resistances in the wiring, solution, and substrate, all of the data were iR-corrected by subtracting the ohmic resistance loss from the overpotential.

Cyclic voltammetry (CV) tests were performed between -0.3 to 0 V at a scanning rate of 100 mV/s for 1000-3000 cycles. Electrochemical impedance spectroscopy (EIS) were recorded with a frequency range of 0.01~10^4 Hz and an amplitude of 5 mV at an overpotential of 0.2 V vs RHE. The onset potential was defined as the potential when the current density (j) reached 1.0 mA/cm^2. The Tafel plots were recorded with the linear regions fitted into the Tafel equation $\eta = b \log(j) + a$, where η, j and b are the overpotential, current density and Tafel slope, respectively. The electrochemically active surface area (ECSA) was estimated based on the electrochemical double-layer capacitance () and mass density. The C_{dl} of the catalytic surface was calculated based on the CV results at 0.4-0.6 V vs RHE using different scan rates (5, 10, 15, 20, 15, 30 mV/s).

Theoretical Calculation

Quantum-chemical calculations were performed using Vienna ab initio simulation package (VASP). Generalized Gradient Approximation (GGA) in the Perdew-Burke-

Ernzerhof (PBE) parametrization was used for description of exchange correlation potential. The s, p electrons in selenium (Se), oxygen (O) and phosphorus (P), the 5d, 6s electrons in tungsten (W) and the 4s, 3d electrons in cobalt (Co) were treated as valence electrons, applying Projector-augmented wave (PAW) atomic potentials.[1] A plane-wave cutoff of 500 eV was used, and a Monkhorst-Pack 4×4×1-point grid was used to sample the Brillouin zone. The calculations were performed using atomic position relaxations, with convergence criteria corresponding to the maximum residual force component of 0.03 eV/Å. Periodic boundary conditions were used in all directions and a vacuum region of 15 Å was introduced along the out-of-plane direction to eliminate spurious interactions among periodic images of 2D structures or along all three directions for individual molecules.

4×4 supercells of 1T' WSe_2 and 1T' WSe_2-O were employed as the main models for the studies of H adsorption. The hydrogen adsorption free energies, ΔG_{H*}, were determined in the same way as in previous studies.[2, 3] The hydrogen adsorption energy is defined as:

$$\Delta E_H = E_{WSe2+H} - E_{WSe2} - 1/2\ E_{H2} \quad (1)$$

where E_{WSe2+H}, E_{WSe2} and E_{H2} refer to the total energies of WSe_2 with adsorbed H*, a clean WSe_2, and gas phase hydrogen molecule. The hydrogen adsorption free energy was calculated at zero potential and pH= 0 as:

$$\Delta G_{H*} = \Delta E_H + \Delta E_{ZPE} - T\Delta S \quad (2)$$

where ΔE_H is the hydrogen adsorption energy, ΔE_{ZPE} is the difference in zero point energy, T is the temperature (300 K) and ΔS is the difference in entropy between H that is adsorbed and in the gas phase, at 101325 Pa. According to previous studies, $\Delta E_{ZPE} - T\Delta S$ is approximately +0.24 eV.[4]

The formation energy, E_f, of the impurity O is defined as the energy needed to insert an O atom into WSe_2 after removing one Se atom.

$$E_f = E_{WSe2-O} - E_{WSe2} + \mu_{Se} - \mu_O \quad (3)$$

where E_{WSe2-O} are the total energy of 2H or 1T' WSe_2 with one O impurity, μ_{Se} is the chemical potential of Se (set equal to the energy per atom of bulk Se), and μ_O is the chemical potential of an O atom (set equal to the energy per atom of O_2). When the

influence of Co and P is considered, $E_{WSe2\text{-}O}$ is replaced by $E_{Co/WSe2\text{-}O}$ or $E_{Co/P/WSe2\text{-}O}$.

Supplementary Figures and Tables

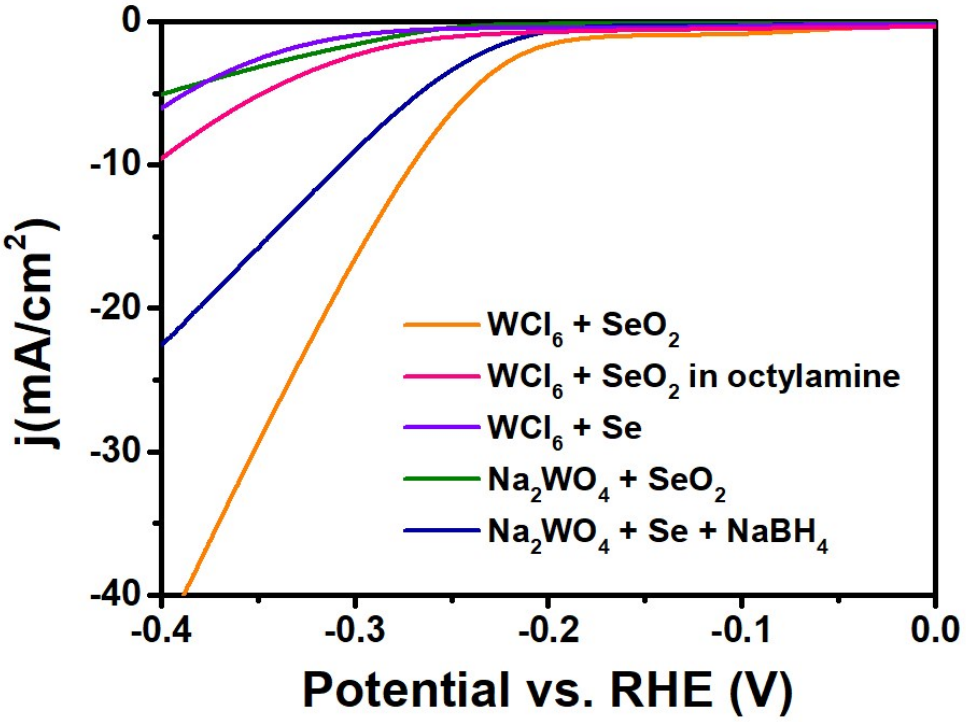

Fig. S1 Polarization curves of WSe_2 synthesized by various precursors.

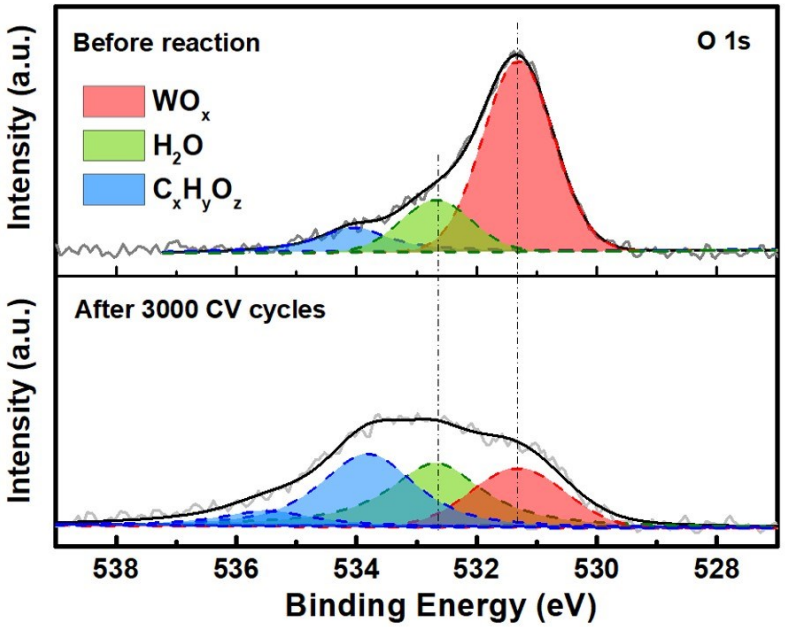

Fig. S2 O 1s XPS spectra of hp-WSe_2 before and after 3000 CV cycles.

The ratio of O attributed to WO_x reduced from 68% to 26% after 3000 CV cycles. Considering the overall O amount in the surface of hp-WSe_2 detected by XPS before and after HER cycles (39.7% and 50.6% respectively), the amount of O belong to WO_x decreased to half of its original value (from 27% to 13%).

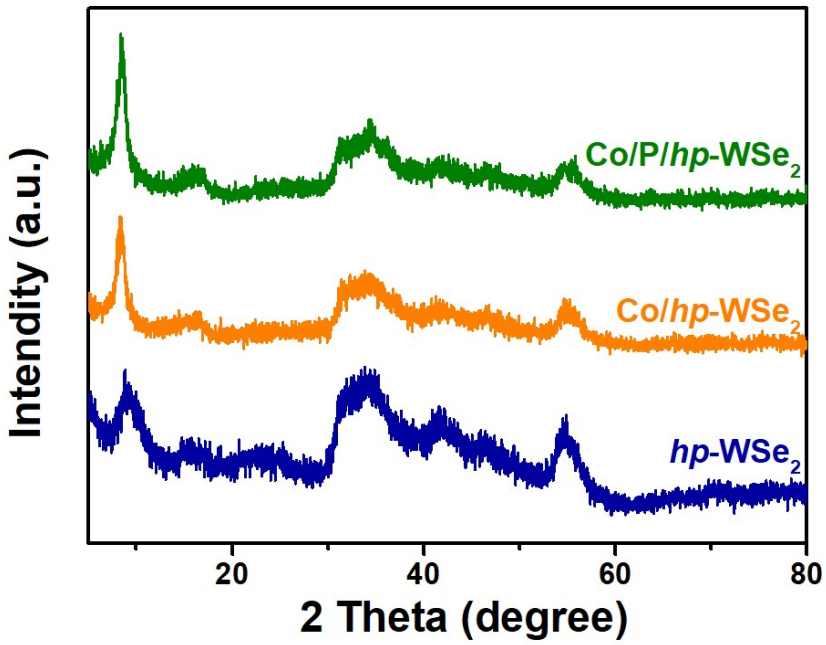

Fig. S3 XRD patterns of *hp*-WSe_2, Co/*hp*-WSe_2 and Co/P/*hp*-WSe_2.

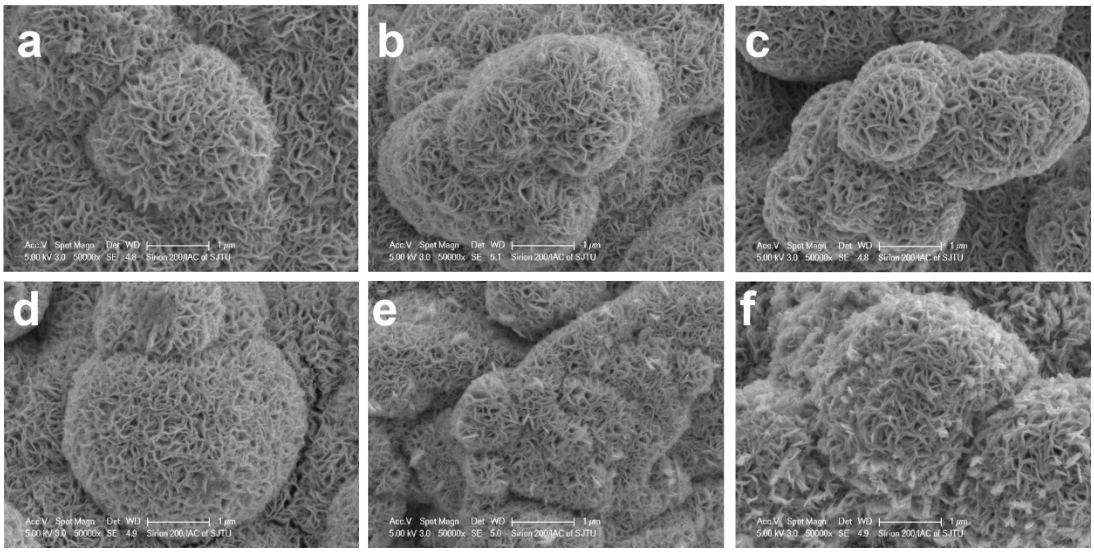

Fig. S4 Typical SEM images of (a) *hp*-WSe_2, (b) Co/*hp*-WSe_2 and (c) Co/P/*hp*-WSe_2 and (d) *hp*-WSe_2, (e) Co/*hp*-WSe_2 and (f) Co/P/*hp*-WSe_2 after 3000 CV cycles at -0.3 to 0 V vs. RHE.

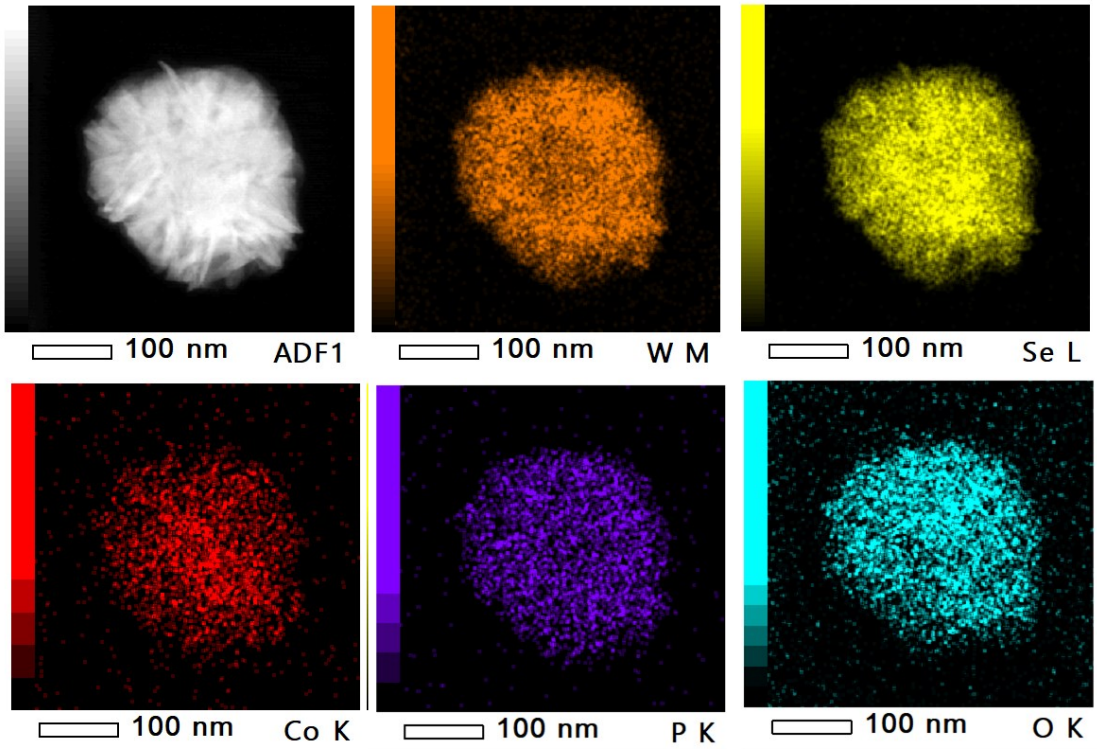

Fig. S5 Elemental mapping results of Co/P/*hp*-WSe_2.

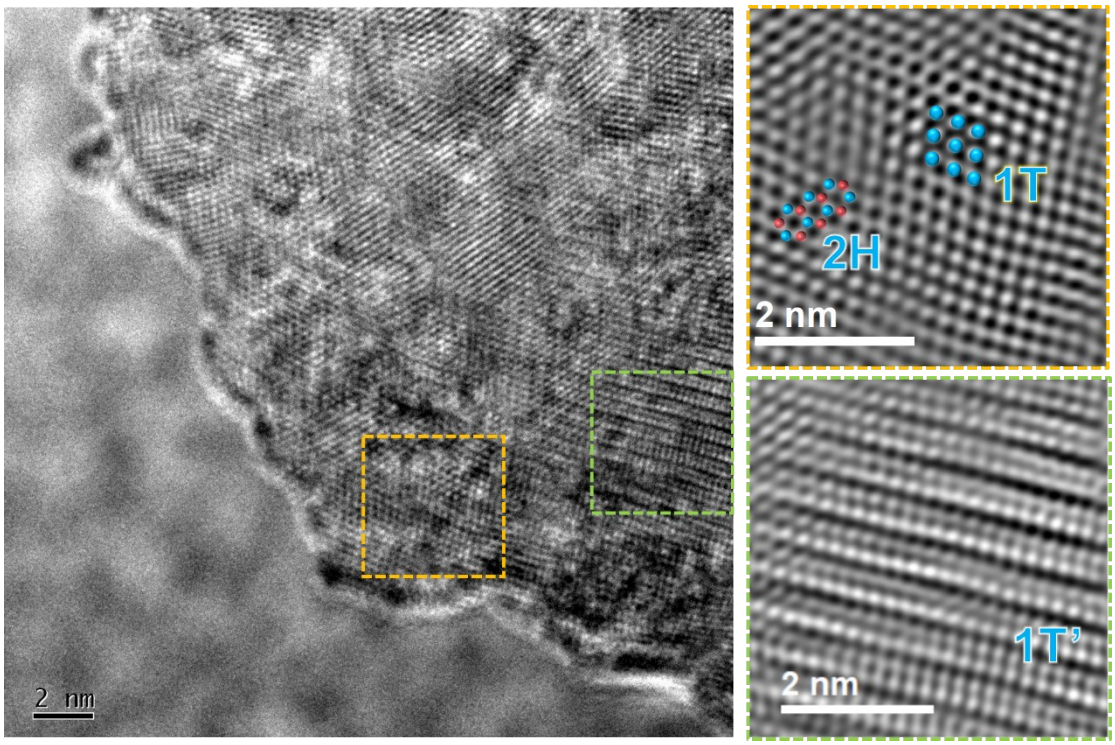

Fig. S6 HRTEM images of Co/P/*hp*-WSe_2

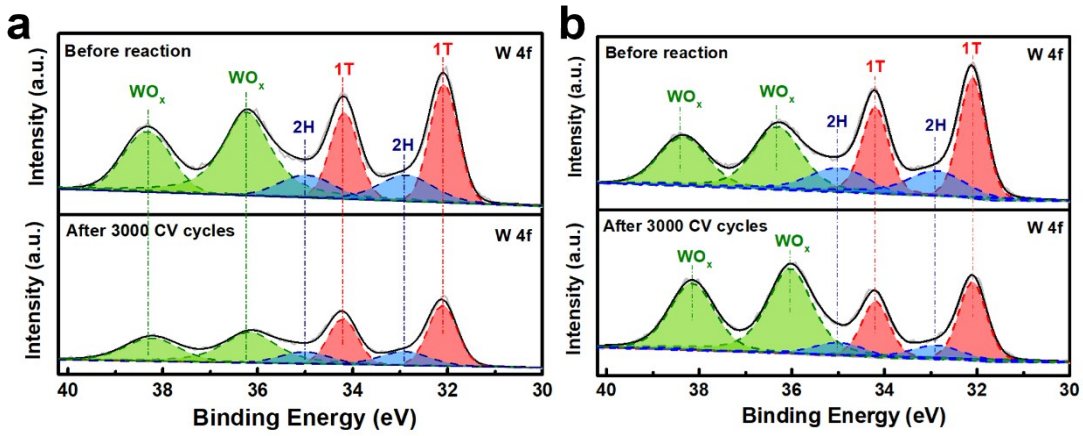

Fig. S7 W 4f XPS spectra of (a) Co/*hp*-WSe_2 and (b) Co/P/*hp*-WSe_2 before and after 3000 CV cycles.

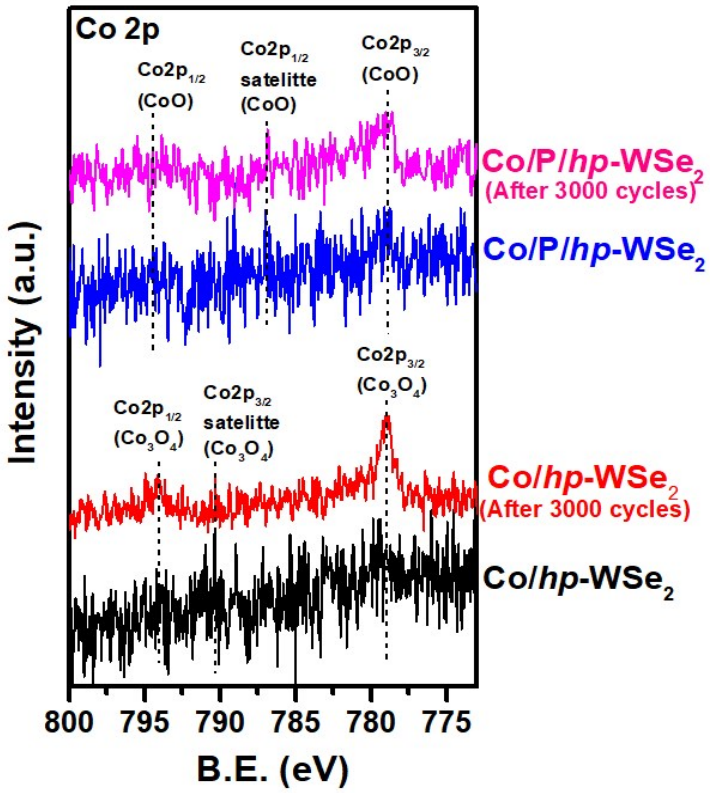

Fig. S8 Co 2p XPS spectra of Co/*hp*-WSe_2 and Co/P/*hp*-WSe_2 before and after 3000 CV cycles

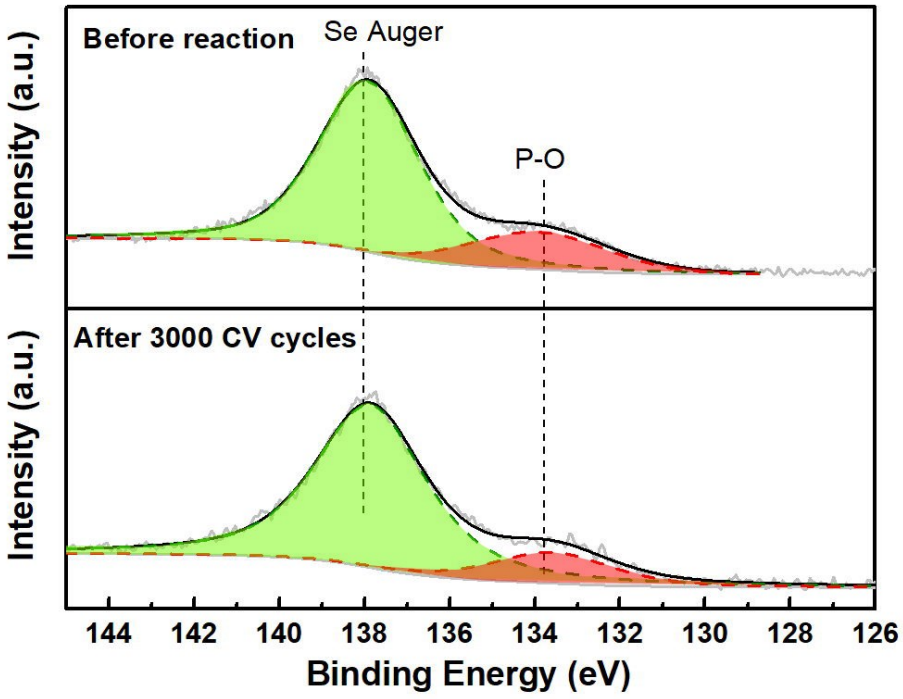

Fig. S9 XPS spectra in P 2p region of Co/P/*hp*-WSe_2 before and after 3000 CV cycles.

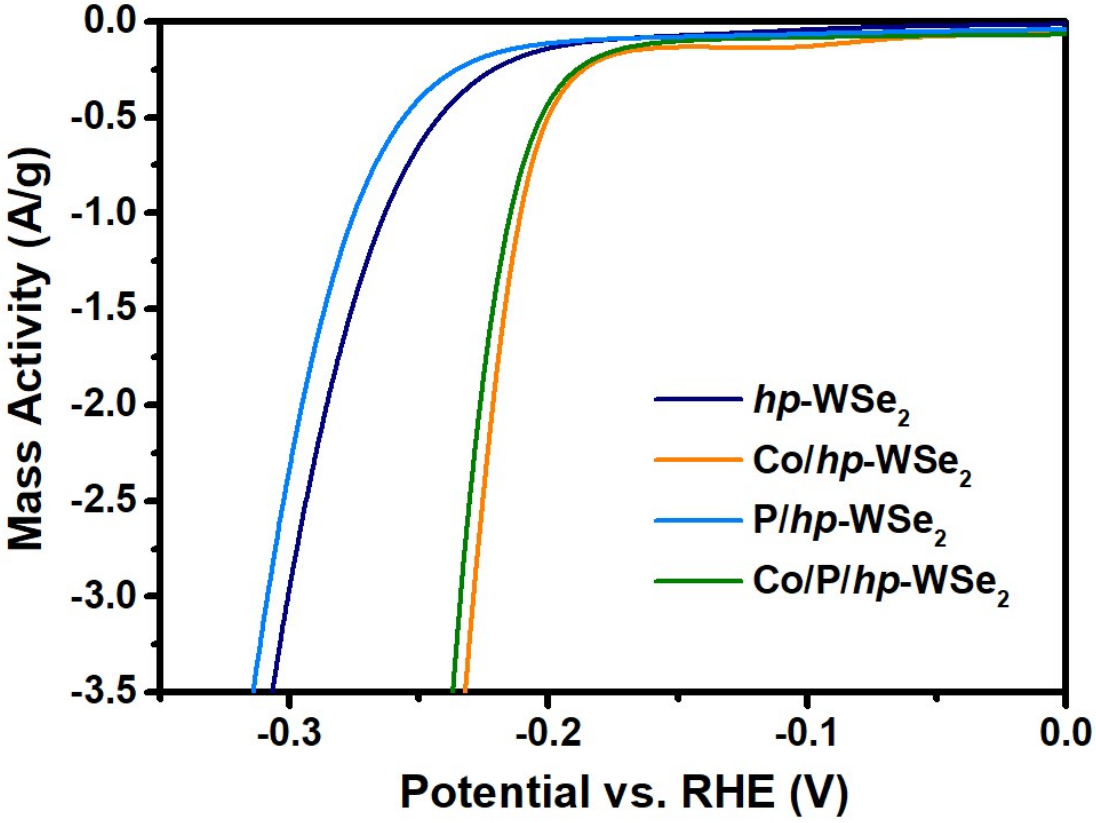

Fig. S10 Mass activities of *hp*-WSe_2, Co/*hp*-WSe_2, P/*hp*-WSe_2 and Co/P/*hp*-WSe_2.

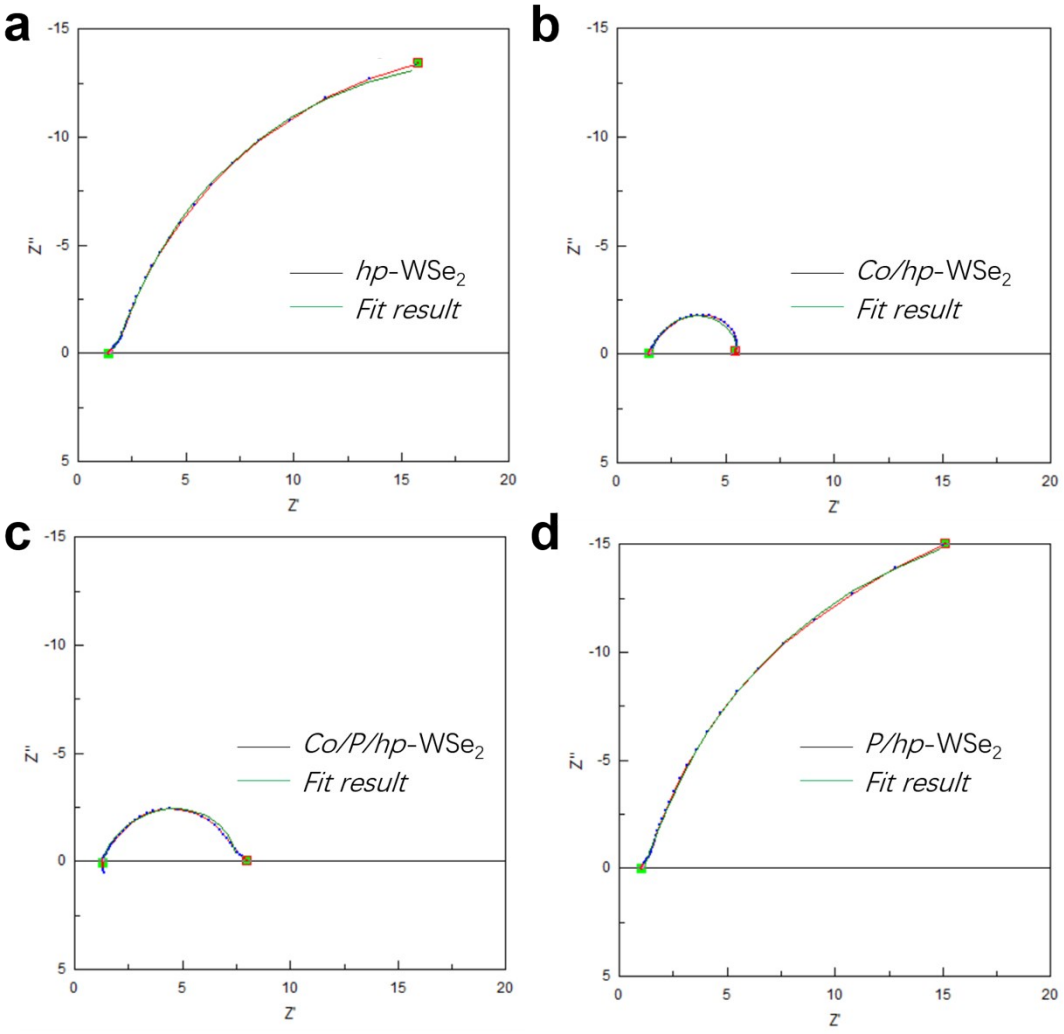

e

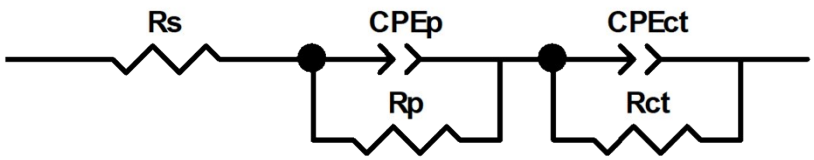

f

Element	Value			
	hp-WSe_2	Co/*hp*-WSe_2	Co/P/*hp*-WSe_2	P/*hp*-WSe_2
Rs	1.44	1.48	1.31	1.06
CPEp-T	0.86	0.10	0.42	0.97
CPEp-P	0.48	0.97	0.99	0.66
Rp	1.24	3.26	2.45	0.34
CPEct-T	0.43	0.20	0.12	0.39
CPEct-P	0.87	0.73	0.82	0.84
Rct	32.53	0.86	3.78	40.97

Fig. S11 The electrochemical impedance spectra and fitting results of (a) *hp*-WSe_2, (b) Co/*hp*-WSe_2, (c) P/*hp*-WSe_2 and (d) Co/P/*hp*-WSe_2; (e) The fitted equivalent circuits and (f) the corresponding data for each sample.

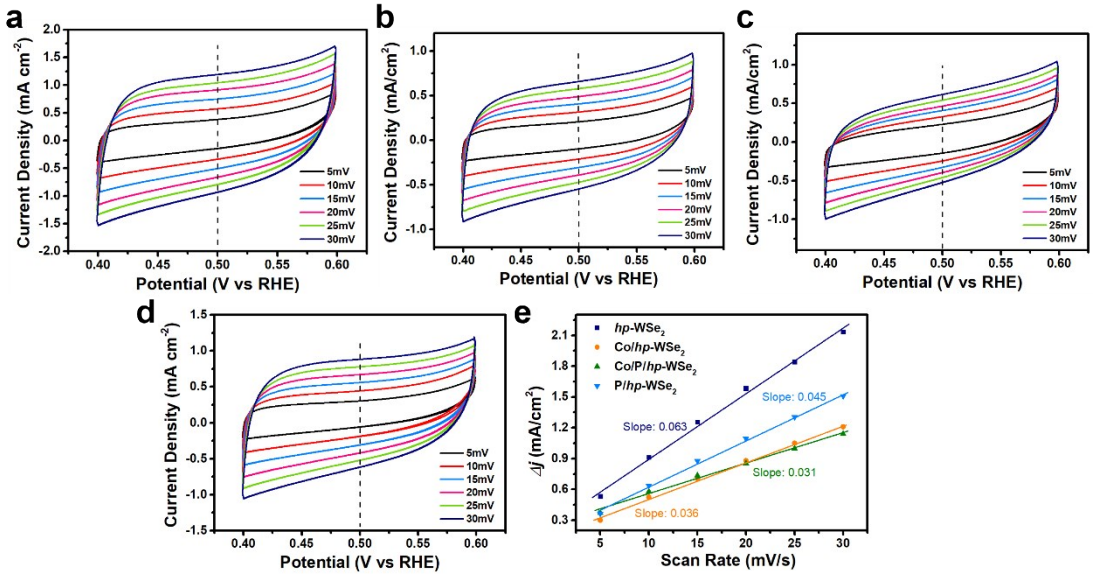

Fig. S12 Cyclic voltammograms in a non-Faradaic region (0.4~0.6 V vs RHE) at scan rates of 5-30 mV/s for (a) *hp*-WSe_2, (b) Co/*hp*-WSe_2, (c) Co/P/*hp*-WSe_2 and (d) P/*hp*-WSe_2; (e) Capacitive $\Delta j = j_a - j_c$ as a function of the scan rate for the samples.

Table S1 HER performance of reported WSe_2 catalysts in 0.5 M H_2SO_4

Sample Name	1T/1T' ratio	η_{10} (mV)	Tafel Slope (mV/dec)	Ref.
WSe_2 nanofilms on carbon fiber paper	N/A	300	77.4	Wang et al., 2013[5]
Bulk or MeLi/BuLi exfoliated WSe_2	2.6~66%	800~700	100~120	Eng et al., 2014[6]
WSe_2 Nanotubes	N/A	~350	99	Xu et al., 2014[7]
$WS_{0.48}Se_{0.52}$ Nanotubes	N/A	~270	105	
BuLi exfoliated WSe_2	<5%	750~800	>240	Ambrosi et al., 2015[8]
WSe_2 on carbon nanofiber	N/A	158-214	98-117	Zou et al., 2015[9]
$W(Se_{0.4}S_{0.6})_2$ nanoflakes grown on carbon nanofiber	N/A	174	108	Zou et al., 2015[9]
3D dendritic WSe_2 on carbon nanofiber mats	N/A	228	80	Zou et al., 2015[10]
Co–WSe_2/rGO	N/A	217	64	Huang et al., 2016[11]
WSe_2 layers on graphene sheets	N/A	180	64	Liu et al., 2016[12]
WSe_2 with Se vacancies	N/A	245	76	Sun et al., 2016[3]
$Mo_{0.57}We_{0.43}Se_2$	N/A	209	76	Meiron et al., 2017[13]
V/Nb/Ta doped WSe_2	~60%	~750	110~130	Chia et al., 2018[14]
Li^+ activated WSe_2 on carbon fiber electrode	N/A	243	116	Henckel et al., 2018[15]
WSe2/rGO hybrid structure	N/A	450	85	Li et al., 2018[16]
Strained Co-doped WSe_2/MWNT	72.1%	174	37	Zhang et al., 2018[17]
1T' WSe_2	100%	510	150	Sokolikova et al., 2019[18]
2H WSe_2 (by annealing 1T' WSe_2 at 500 °C)	0%	640	232	
10% Ni–WSe_2	N/A	259	86	Kadam et al., 2020 [4]
Co/P/*hp*-WSe_2	64%	225	39	Present Work

Reference

1. G. Kresse and D. Joubert, *Phys. Rev. B*, 1999, **59**, 1758-1775.
2. H. Li, C. Tsai, A. L. Koh, L. Cai, A. W. Contryman, A. H. Fragapane, J. Zhao, H. S. Han, H. C. Manoharan and F. Abild-Pedersen, *Nat. Mater.* , 2016, **15**, 48-53.
3. Y. Sun, X. Zhang, B. Mao and M. Cao, *Chem. Commun.*, 2016, **52**, 14266-14269.
4. S. R. Kadam, A. N. Enyashin, L. Houben, R. Bar-Ziv and M. Bar-Sadan, *J. Mater. Chem. A*, 2020, **8**, 1403-1416.
5. H. Wang, D. Kong, P. Johanes, J. J. Cha, G. Zheng, K. Yan, N. Liu and Y. Cui, *Nano Lett.*, 2013, **13**, 3426-3433.
6. A. Y. Eng, A. Ambrosi, Z. Sofer, P. Simek and M. Pumera, *ACS Nano*, 2014, **8**, 12185-12198.
7. K. Xu, F. Wang, Z. Wang, X. Zhan, Q. Wang, Z. Cheng, M. Safdar and J. He, *ACS Nano*, 2014, **8**, 8468-8476.
8. A. Ambrosi, Z. Sofer and M. Pumera, *Chem. Commun.*, 2015, **51**, 8450-8453.
9. M. Zou, J. Chen, L. Xiao, H. Zhu, T. Yang, M. Zhang and M. Du, *J. Mater. Chem. A*, 2015, **3**, 18090-18097.
10. M. Zou, J. Zhang, H. Zhu, M. Du, Q. Wang, M. Zhang and X. Zhang, *J. Mater. Chem. A*, 2015, **3**, 12149-12153.
11. Y. Huang, Z. Ma, Y. Hu, D. Chai, Y. Qiu, G. Gao and P. Hu, *RSC Adv.*, 2016, **6**, 51725-51731.
12. Z. Liu, H. Zhao, N. Li, Y. Zhang, X. Zhang and Y. Du, *Inorg. Chem. Front.*, 2016, **3**, 313-319.
13. O. E. Meiron, V. Kuraganti, I. Hod, R. Bar-Ziv and M. Bar-Sadan, *Nanoscale*, 2017, **9**, 13998-14005.
14. X. S. Chia, N. A. A; Sofer, Z; Luxa, J; Pumera, M., *Chem. Eur. J.*, 2018, **24**, 3199 –3208.
15. D. A. Henckel, O. M. Lenz, K. M. Krishnan and B. M. Cossairt, *Nano Lett.* , 2018, **18**, 2329-2335.
16. J. Li, P. Liu, Y. Qu, T. Liao and B. Xiang, *International Journal of Hydrogen Energy*, 2018, **43**, 2601-2609.
17. G. Zhang, X. Zheng, Q. Xu, J. Zhang, W. Liu and J. Chen, *J. Mater. Chem. A*, 2018, **6**, 4793-4800.
18. M. S. Sokolikova, P. C. Sherrell, P. Palczynski, V. L. Bemmer and C. Mattevi, *Nat. Comm.*, 2019, **10**, 712.